Title	Annealing effects on the optical properties of a GaInNAs double barrier quantum well infrared photodetector
Author(s)	Ma, B. S.; Fan, Weijun; Dang, Y. X.; Cheah, Weng Kwong; Yoon, Soon Fatt
Citation	Ma, B. S., Fan, W., Dang, Y. X., Cheah, W. K.,& Yoon, S. F. (2007). Annealing effects on the optical properties of a GaInNAs double barrier quantum well infrared photodetector. Applied physics letters, 91(4), 041905.
Date	2007
URL	http://hdl.handle.net/10220/18119
Rights	

Annealing effects on the optical properties of a GaInNAs double barrier quantum well infrared photodetector

B. S. Ma, W. J. Fan,[a] Y. X. Dang, W. K. Cheah, and S. F. Yoon
School of Electrical and Electronic Engineering, Nanyang Technological University, Singapore 639798

(Received 3 May 2007; accepted 30 June 2007; published online 25 July 2007)

Annealing effects in a GaInNAs/AlAs/AlGaAs double barrier quantum well infrared photo detector were studied by x-ray diffraction, photoluminescence (PL), and photoluminescence excitation (PLE) spectroscopy. After annealing at 650 °C, the GaInNAs PL peak shows stronger PL intensity and blueshift of 40 meV mainly due to the group-III interdiffusion. As the annealing temperature increases to 825 °C, the blueshift decreases from 40 to 15 meV due to the nitrogen substitutional-interstitional kickout effect, Al/Ga interdiffusion at the AlAs/AlGaAs interface, and strain reduction. After annealing, the difference between the PLE peak energy and the detection energy decreases with increasing detection energy because of the redistribution of elemental concentrations. © *2007 American Institute of Physics*. [DOI: 10.1063/1.2762290]

The past decades have witnessed intensive experimental and theoretical research interest in the dilute nitride semiconductors, such as GaAsN and GaInNAs (GINA), due to their particular electronic and optical properties and various optoelectronic applications. The incorporation of a few percent of nitrogen induces a significant decrease in the band gap and a large conduction band offset.[1] The GaInNAs/GaAs and GaInNAs/AlGaAs conduction band discontinuity can be as large as 600 meV and 1 eV, respectively.[2,3] Thus it is possible to apply the intersubband transitions in a Ga(In)NAs quantum well to quantum well infrared photodetectors (QWIPs) in the near- and mid-infrared wavelength range. Practically, the GaAsN/AlAs/AlGaAs double barrier quantum well infrared photo detectors (DBQWIPs) operating in the wavelength range of 2.5–4 and 1.64–1.67 μm have been grown.[4,5] On the other hand, the incorporation of nitrogen leads to the deterioration in optical and structural properties of the material. Thus, postgrowth rapid thermal annealing (RTA) is always necessary to improve the optical and crystalline quality. Unfortunately, an unfavorable blueshift in the photoluminescence (PL) peak energy is always observed after annealing.[6] In this letter, the annealing effects in a GaInNAs/AlAs/AlGaAs DBQWIP were investigated using x-ray diffraction (XRD), PL, and photoluminscence excitation (PLE) spectroscopy. Several novelties, such as a worse XRD resolution in the annealed samples than the as-grown one, the decrease of annealing induced blueshift with increasing annealing temperature, and the reduction in the difference between the PLE peak energy and the detection energy with increasing detection energy in the annealed sample, were observed and explained using the $k \cdot p$ calculations.

The GINA QWIP was grown on a semi-insulating (001)-oriented GaAs substrate in a Riber MBE 32 solid-state molecular beam epitaxy system with a N_2 radio frequency plasma nitrogen source. The active region of the studied sample contains ten periods of multi-quantum-well (MQW) structures with a 2.3 nm thick Si-doped (1×10^{18} cm^{-3}) $In_{0.288}Ga_{0.712}As_{0.997}N_{0.013}$ quantum well sandwiched between two undoped 1.3 nm thick AlAs inner barriers and further separated by 13 nm thick $Al_{0.3}Ga_{0.7}As$ outer barrier layers in each period. The whole ten-period region was buffered by a 0.3 μm thick Si-doped (2×10^{18} cm^{-3}) GaAs bottom contact layer and capped by a 0.5 μm thick Si-doped (2×10^{18} cm^{-3}) GaAs top contact layer. The AlAs and AlGaAs barriers and the GINA wells were all grown at 460 °C and the contact layers at 580 °C. In the RTA experiments, 6×6 mm^2 wafer pieces were cut from the main sample and capped by GaAs wafers to prevent the As evaporation at the surface. Annealing was carried out under the N_2 environment at 650–825 °C for a short duration of 20 s. The pieces of the sample annealed at different annealing temperatures are different.

The XRD rocking curves, obtained from the $\omega-2\theta$ scans in the (004) plane for the QWIP structures before and after RTA at different temperatures, are shown in Fig. 1. The XRD simulation for the as-grown samples is illustrated by the dashed line in Fig. 1. In the measured XRD curve of the as-grown sample, the clear satellite peaks indicate good structural quality. After annealing at 650 and 700 °C, the

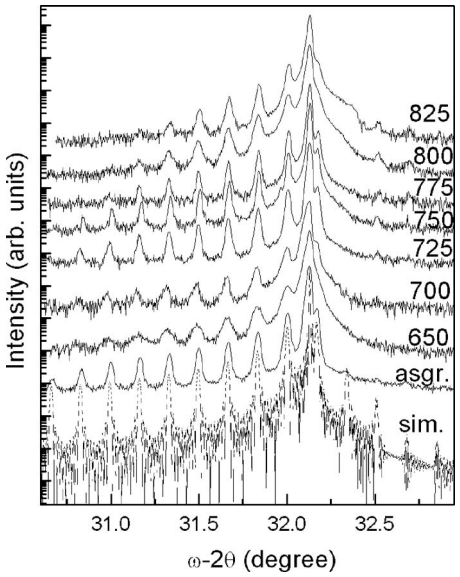

FIG. 1. XRD rocking curves of the as-grown and annealed QWIP structures (solid line) and the dynamical simulation for the as-grown sample (dashed line). The curves are vertically shifted for clarity. The digits beside the curves are the annealing temperatures.

[a]Electronic mail: ewjfan@ntu.edu.sg

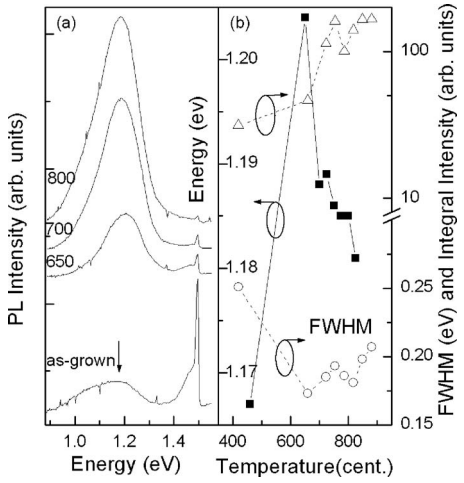

FIG. 2. (a) Photoluminescence spectra of the as-grown and annealed GINA QWIP structures measured at 5 K and (b) the variations with annealing temperature of the peak energy (filled squares), FWHM (empty circles), and the integral intensity (empty triangles) of the main PL peak. The spectra are vertically shifted for clarity. The digits beside the spectra are the corresponding annealing temperature.

satellite peaks broaden and weaken. This suggests that the elemental compositions and/or layer profiles change in the MQW upon annealing. When annealing temperature increases, the satellite peaks get sharper and stronger. The larger number and better resolution of the satellite peaks are observed at 725 and 750 °C, but they are still a little inferior to those of the as-grown sample. When annealing temperature increases further, however, these satellite peaks turn fewer, weaker, and broader again.

For the PL measurements, the 514.5 nm Ar^+ laser line was used as excitation. The luminescence signals were dispersed by a Spex 0.75 m monochromator and then detected by a liquid nitrogen cooled Ge photodetector using a standard lock-in technique. Figure 2(a) depicts the PL spectra measured at 4.8 K of the as-grown and annealed QWIP samples. The as-grown sample shows two PL features at 1.17 and 1.5 eV. The stronger and sharper peak at 1.5 eV is related to GaAs. Its low-energy shoulder results from the heavy silicon doping. The weaker and much broader peaks at 1.17 eV are attributed to the band-gap transition in the GINA quantum well. The long tail at the low-energy side of the GINA peak, which features dilute nitrides, arises not only from localized states due to alloy fluctuations,[7] but also from impurity and defect traps induced by silicon and nitrogen doping, such as interstitial nitrogen and other nitrogen complexes.[8] The latter dominates the former since the tail shape is far from an exponential one characterizing the potential fluctuations.[7]

To verify the origin of the PL peak, we performed calculations using the $k\cdot p$ model.[9] The strain effects have been considered in the $k\cdot p$ Hamiltonian. The band-gap energy of $Ga_1-xIn_xN_yAs_{1-y}$ is calculated using the band anticrossing model as follows:[10]

$$E_g(\mathrm{In}_x\mathrm{Ga}_{1-x}\mathrm{As}_{1-y}\mathrm{N}_y) = \frac{1}{2}\{E_g(\mathrm{In}_x\mathrm{Ga}_{1-x}\mathrm{As}) + E_N - \sqrt{[E_g(\mathrm{In}_x\mathrm{Ga}_{1-x}\mathrm{As}) - E_N]^2 + 4V_{NC}^2 y}\}, \quad (1)$$

where E_g(InGaAs), E_N and V_{NC} are the band-gap energies of InGaAs at Γ point, the energy of the isolated nitrogen level in the InGaAs host material, and the coefficient describing the coupling strength between E_N and the InGaAs conduction band, respectively. The effective mass and the conduction band offset ratio are chosen to be 0.09 and 0.8, respectively.[11,12] The calculated interband transition energy (from the ground level in the conduction band to the first heavy-hole state in the valence band) in the GINA well is 1.18 eV, as indicated by the arrow in Fig. 2(a). The calculation result agrees well with the above assignment of the PL peak.

After RTA for 20 s, the GINA PL peak gets much stronger in intensity and dominates the GaAs peak, and show a more symmetric shape with a weaker low-energy tail, as shown in Fig. 2(a). These changes indicate a strong enhancement of the radiative recombination efficiency in the GINA quantum well due to a significant annealing induced decrease of nonradiative centers. The full width at half maximum (FWHM) gets a little smaller but is still as large as 180–200 meV due to silicon doping and the redistribution of the elemental concentrations in the MQW as discussed later in the PLE spectra. The improvement in optical efficiency of GINA is accompanied by a large blueshift of ~40 meV upon annealing at 650 °C. Considering the weakening and broadening of the XRD satellite peaks, the atom interdiffusion, especially the group-III atom interdiffusion,[13] which changes the elemental concentration profiles and diminishes the periodicity,[14] is a dominant mechanism underlying this blueshift.

When the annealing temperature increases from 650 to 825 °C, the blueshift does not continue, as shown in Fig. 2(b), and the GINA PL peak moves to the lower-energy side. Such an annealing induced redshift or suppressed blueshift in PL energy mainly originated from three effects. Firstly, when the annealing temperature is lower than 750 °C, the kickout effect of substitutional arsenic atoms by interstitial nitrogen atoms narrows the band gap.[15] This substitutional-interstitional swap of nitrogen atoms improves the crystalline quality,[15] and thus the XRD features show the better resolution at 725–750 °C. Secondly, the atom interdiffusion, especially the outdiffusion of indium from the well, reduces the compressive strain in the GINA well and therefore the heavy-hole band-gap transition energy decreases. Thirdly, at higher annealing temperatures, especially above 800 °C, the Al/Ga interdiffusion at the AlAs/AlGaAs interface, which is very small at 650–750 °C, becomes significant due to a large activation energy of 3.6–6 eV,[16,17] in comparing with that of 0.8–1.93 eV of the In/Ga interdiffusion.[14] In the double barrier structures, thin AlAs barriers increase the carrier confinement energy in the well.[18] The Al/Ga interdiffusion, however, reduces the AlAs barrier's height so that the confinement energy and interband transition energy decrease. In addition, the point defects in the AlAs and AlGaAs layers grown at the low growth temperature of 460 °C enhance this Al/Ga interdiffusion. Due to the Al/Ga and other atom interdiffusions, the XRD patterns get broader and weaker again at higher temperatures above 750 °C. After all, the atom interdiffusion at higher temperatures does not result in apparent structure degradation, and thus the PL peaks show little change in intensity and FWHM, as can be seen in Fig. 2(b).

In the PLE measurements, the tunable light source was provided by a 250 W tungsten-halogen lamp dispersed by a

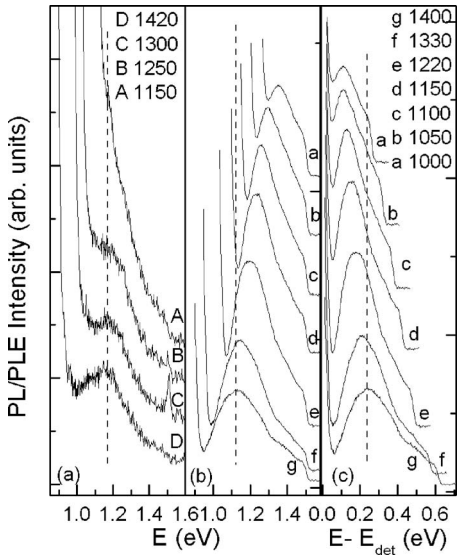

FIG. 3. PLE spectra measured at 8 K for (a) the as-grown QWIP samples and (b) the sample annealed at 750 °C and (c) plotted against $E-E_{\mathrm{det}}$ for the annealed sample. In (a), spectra A, B, C, and D were obtained at the detection wavelengths of 1150, 1250, 1350, and 1420 nm, respectively. In (b) and (c), the detection wavelengths for spectra a,b,…,g are 1000, 1050, … , 1400 nm, respectively. The vertical dashed line indicates the peak energy positions of spectra D and g.

TRIAX 320 monochromator. The luminescence was analyzed by another TRIAX 320 monochromator and detected by a thermoelectrically cooled InGaAs detector. The PLE spectra of the as-grown sample and the sample annealed at 750 °C have been measured at 8 K at different detection wavelengths, as shown in Fig. 3. The peaks at 1.5 eV in the PLE spectra of the as-grown sample and the steplike features at 1.5 eV in those of the annealed sample are related to the band-edge transition of GaAs. The PLE features with energy lower than 1.5 eV are related to the MQW region. Typically, the PLE spectra of GaInNAs/GaAs quantum wells are characterized by a steplike profile and the independence of spectra on the detection wavelength.[19] However, the GINA QWIP structure studied here shows some interesting differences. Firstly, there is only a broad peak without clear steplike features mainly due to the defect and impurity centers. Secondly, the PLE peaks of the as-grown and annealed samples show distinctly different dependence on the detection wavelength. For the as-grown sample, the PLE peak shifts little with detection wavelength, which is typical for a normal GaInNAs/GaAs QW.[19] However, the PLE peaks of the annealed sample show sensitive dependence on the detection wavelength. As the detection wavelength increases or the detection energy, E_{det}, decreases, the energy of the PLE peak, E, decreases. This phenomenon has also been observed in a GaInNAs/GaAs structure consisting of phase-separated quantum dots.[20] However, it is not reasonable to ascribe our observation to the subensembles of quantum dots in the well, which is only 2.3 nm wide, and the fact that $E-E_{\mathrm{det}}$ of the PLE peak decreases with the increase of E_{det}, as illustrated in Fig. 3(c), is contrary to the quantum size effect in the quantum dots.[20,21] In our opinion, the explanation lies in the elemental concentration redistribution in the annealed samples. As mentioned above, the as-grown sample exhibits the best periodicity leading to the best XRD resolution. Upon annealing, the atom interdiffusion varies the elemental concentration and layer profile in each individual quantum well. Therefore, the elemental concentration is not a constant, and the layer profile of the GINA well is not a rectangle but can be considered to be composed of quantum wells with different well widths. In addition, the diversity of the concentration and layer profile exists among different quantum wells after annealing.[14] Such redistributions of elemental concentrations and diversity give rise to a broad distribution in energy level and transition energy, as evidenced by the large FWHM of the PL peaks. We assigned the PLE peaks mainly to the transitions from the first electron sublevel, e1, to the first light-hole sublevel, lh1. The excitation photons only excite carriers resonantly in quantum wells with particular indium concentration and well thickness defined by the detection energy. These carriers at the lh1 levels then relax inside the particular wells to the ground heavy-hole sublevel, hh1, where they recombine radiatively. Our calculations using the $k\cdot p$ method show that when the indium and/or the GINA well width vary, the energy difference between the lh1 and hh1 sublevels, $E_{\mathrm{hh1}}-E_{\mathrm{lh1}}$, exhibits a monotone decrease with the heavy-hole interband transition energy E_1-E_{hh1}, where E_1, E_{hh1} and E_{lh1} are the energies of the e1, hh1, and lh1 levels. Therefore the negative correlation between $E_{\mathrm{hh1}}-E_{\mathrm{lh1}}$ and E_1-E_{hh1} is visualized by that between the $E-E_{\mathrm{det}}$ of the PLE peak and E_{det}.

The authors would like to acknowledge the support for this work from A*STAR (Grant No. 042 101 0077). One of the authors, B.S.M., would like to thank Deny Sentosa for her help with the annealing process.

[1] H. P. Xin, C. W. Tu, and M. Geva, Appl. Phys. Lett. **75**, 1416 (1999).
[2] J.-Y. Duboz, J. A. Gupta, M. Byloss, G. C. Aers, H. C. Liu, and Z. R. Wasilewski, Appl. Phys. Lett. **81**, 1836 (2002).
[3] J. Y. Duboz, Phys. Rev. B **75**, 045327 (2007).
[4] A. Guzmán, E. Luna, J. Miguel-Sánchez, E. Calleja, and E. Munoz, Infrared Phys. Technol. **44**, 377 (2003).
[5] E. Luna, M. Hopkinson, J. M. Ulloa, A. Guzman, and E. Munoz, Appl. Phys. Lett. **83**, 3111 (2003).
[6] J.-M. Chauveau, A. Trampert, K. H. Ploog, and E. Tournié, Appl. Phys. Lett. **84**, 2503 (2004).
[7] A. Polimenti, F. Masia, G. Baldassarri Höger von Högersthal, and M. Capizzi, in *Dilute Nitride Semiconductors*, edited by M. Henimi (Elsevier, Amsterdam, 2005), p. 225.
[8] W J. Fan, S. F. Yoon, T. K. Ng, S. Z. Wang, W. K. Loke, R. Liu, and A. Wee, Appl. Phys. Lett. **80**, 4136 (2002).
[9] S. T. Ng, W. J. Fan, Y. X. Dang, and S. F. Yoon, Phys. Rev. B **72**, 115341 (2005).
[10] W. Shan, W. Walukiewicz, J. W. Ager III, E. E. Haller, J. F. Geisz, D. J. Friedman, J. M. Olson, and S. R. Kurtz, Phys. Rev. Lett. **82**, 1221 (1999).
[11] R. Kudrawiec, M. Gladysiewicz, J. Misiewicz, F. Ishikawa, and K. H. Ploog, Appl. Phys. Lett. **90**, 041916 (2007).
[12] Z. Pan, L. H. Li, Y. W. Lin, B. Q. Sun, D. S. Jiang, and W. K. Ge, Appl. Phys. Lett. **78**, 2217 (2001).
[13] Z. Pan, L. H. Li, W. Zhang, Y. W. Lin, R. H. Wu, and W. Ge, Appl. Phys. Lett. **77**, 1280 (2000).
[14] G. Mussier, L. Däweritz, and K. H. Ploog, Appl. Phys. Lett. **87**, 081903 (2005).
[15] W. K. Loke, S. F. Yoon, S. Z. Wang, T. K. Ng, and W. J. Fan, J. Appl. Phys. **91**, 4900 (2002).
[16] T. E. Schlesinger and T. Kuech, Appl. Phys. Lett. **49**, 519 (1986).
[17] L. L. Chang and A. Koma, Appl. Phys. Lett. **29**, 138 (1976).
[18] M. Colocci, M. Gurioli, J. Martinez-Pastor, B. Chastaingt, C. Deparis, G. Neu, and J. Massies, Proc. SPIE **1985**, 592 (1993).
[19] H. D. Sun, A. H. Clark, S. Calvez, M. D. Dawson, K. S. Kim, T. Kim, and Y. J. Park, Appl. Phys. Lett. **87**, 021903 (2005).
[20] H. D. Sun, A. H. Clark, S. Calvez, M. D. Dawson, P. Gilet, L. Grenouillet, and A. Million, J. Appl. Phys. **97**, 033517 (2005).
[21] D. J. Norris, A. Sacra, C. B. Murray, and M. G. Bawendi, Phys. Rev. Lett. **72**, 2612 (1994).